SCIENTIFIC Publishing Limited

New Energy Exploitation and Application

https://ojs.ukscip.com/index.php/neea

Article

Sensitivity of Neutron-Induced Cross Sections to Pre-Equilibrium Modelling in EMPIRE 3.2.3 Code

Abel Blessing Olorunsola [1,*], Abdullahi Mohammed Evuti [2], Damilola Abubakar Atere [1], Mudashir Abdulrauf [1] and Matthew Inalegwu Amanyi [3]

[1] Department of Physics, Faculty of Science, University of Abuja, Abuja 900106, Nigeria

[2] Department of Nuclear Engineering, Faculty of Engineering, University of Abuja, Abuja 900106, Nigeria

[3] Department of Physics, Faculty of Science, Federal University of Health Sciences, Otukpo 972261, Nigeria

[*] Correspondence: abel.olorunsola@uniabuja.edu.ng

Received: 30 January 2026; **Revised:** 28 April 2026; **Accepted:** 18 May 2026; **Published:** 26 May 2026

Abstract: Modelling of neutron-induced reaction cross sections is essential for applied nuclear science and nuclear data evaluation. In this study, excitation functions for the reactions $^{32}S(n,p)^{32}P$, $^{35}Cl(n,\alpha)^{32}P$, and $^{35}Cl(n,p)^{35}S$ were investigated from threshold energies up to 20 MeV. The calculations were performed using the EMPIRE 3.2.3 nuclear reaction code with different pre-equilibrium model options, namely MSD (Multi-Step Direct), MSC (Multi-Step Compound), PCROSS (Pre-equilibrium cross section), and HMS (Hybrid Monte Carlo Simulation). The theoretical results were compared with available experimental data over a broad energy range up to 20 MeV. The calculated cross sections show good agreement with experimental data near threshold energies, indicating the dominance of the compound nucleus mechanism in this region. However, as the incident neutron energy increases above approximately 5 MeV, noticeable discrepancies emerge among the model predictions, reflecting differences in the treatment of pre-equilibrium processes. In particular, the PCROSS model tends to produce relatively higher cross sections in the energy region between 7 MeV and 12 MeV, where multi-step pre-equilibrium effects become more significant. Overall, the results demonstrate that the choice of pre-equilibrium model has a substantial impact on the predicted cross sections. This study highlights the sensitivity of neutron-induced reaction calculations to reaction-mechanism inputs and provides useful guidance for the appropriate selection of model options within the EMPIRE framework for nuclear data evaluation and related applications.

Keywords: Energy-Dependent; EMPIRE 3.2.3; Preequilibrium Emission; Sensitivity Analysis; Sulphur; Chlorine Isotopes

1. Introduction

Accurate neutron-induced reaction cross-section data are fundamental to a wide range of applications in nuclear science and technology, including: radiation shielding, production of radioisotopes, reactor design, nuclear medicine, and the study of geological environments [1]. Experimental cross-section data are sparse, inconsistent, or unavailable; in many cases does not cover the energy range of interest [2–4]. Therefore, supplementing the theoretical models with measurements plays an important role by providing evaluated data for nuclear data libraries. Modern reaction codes, such as EMPIRE, TALYS, and CoH_3 reaction codes, are used widely for this purpose, since their predictive power depends strongly on the chosen reaction mechanism and the underlying physics of the nuclear structure [5–7]. In parallel to nuclear reaction codes, machine learning approaches are also emerging as

powerful tools for nuclear data prediction, as recently demonstrated for fission product yields [8].

Neutron-induced reactions on light and medium-mass nuclei provide a precise test of reaction models from the theoretical perspective since multiple reaction mechanisms contribute across the energy range [9]. At low incident energies, the reaction is predominantly governed by compound nucleus formation, which is well described by the Hauser–Feshbach theory [10]. However, as neutron energy increases, the pre-equilibrium processes are predominant for particle-emission channels, especially (n,p) and (n,α). The relative contributions of the reaction mechanisms are influenced by the sensitivity of the chosen optical-model potentials, as well as the compound nucleus parameters (such as level density and gamma-ray strength), and the pre-equilibrium models [11,12]. Different modelling options led to different predictions within the given EMPIRE reaction code. Most especially as the incident energy increases.

Several in-built models' options are provided in the EMPIRE 3.2.3 statistical reaction code that differ in the treatment of collective enhancement, level density, and preequilibrium emission. For preequilibrium emission, the Multi-Step Direct (MSD), Multi-Step Compound (MSC), Pre-equilibrium cross section (PCROSS), and Hybrid Monte Carlo Simulation (HMS) model options were designed for predictive capability improvement for a wide range of energies, and their performance varies from the reaction type and target nucleus [12,13]. Comparisons of these model options against experimental data are important in systematically identifying the models' strengths and limitations, and for guiding their use in nuclear reaction data evaluation [14].

This work presents a comprehensive sensitivity of neutron-induced cross sections to pre-equilibrium modelling using the EMPIRE 3.2.3 model options for ^{32}S(n,p)^{32}P, ^{35}Cl(n,a)^{32}P, and ^{35}Cl(n,p)^{35}S reactions. Calculated cross sections were compared with available experimental data over the incident neutron energy range from threshold to 20 MeV. Due to the relevance for fundamental and applied contexts, the isotopes of sulphur and chlorine were of particular interest. Neutron-induced ^{32}S and ^{35}Cl targets for the production of ^{32}P and ^{35}S are important beta-emitting radionuclides that are relevant to agricultural, biological tracing, and medical research [15]. Chlorine isotope plays an important role in molten salt reactor design, reaction rate calculation for new astrophysics [16–18]. In particular, this study focuses on understanding the energy-dependent discrepancies among EMPIRE 3.2.3 preequilibrium model options, and the differences are linked with the underlying physical assumptions of each model. The study provides a unified assessment of EMPIRE 3.2.3 model performance within the preequilibrium mechanism and offers guidance for future nuclear data evaluations involving sulphur and chlorine isotopes.

2. Theoretical Calculation

Theoretical EMPIRE 3.2.3 nuclear reaction code was used to investigate neutron-induced reactions on ^{32}S and ^{35}Cl targets for the reaction channels of ^{32}S(n,p)^{32}P, ^{35}Cl(n,a)^{32}P, and ^{35}Cl(n,p)^{35}S from threshold up to 20 MeV neutron energies.

The optical model was treated in EMPIRE as the sum of the elastic and absorption cross secti ons, calculated using the inbuilt ECIS06 code [19].

$$\sigma_{tot} = \sigma_{el} + \sigma_a = \frac{\pi}{k^2} \sum_j (2j+1)(1 - ReS_j) \tag{1}$$

where σ_{tot} is the total cross-section, σ_{el} is the elastic scattering cross-section, and σ_a is the absorption cross-section. k is the wave number of the incident neutron, j is the total angular momentum quantum number, and S_j represents the scattering matrix element for each partial wave.

This expression in Equation (1) accounts for flux loss due to both scattering and absorption of the incident plane wave.

The formation of compound nucleus decay is dominated at low incident energies. The reactions described using the Hauser–Feshbach formalism [10].

$$\sigma_{\mathrm{CN}}^{a\to b}(E) = \sum_{J,\pi} \frac{\pi}{k^2} \frac{(2J+1)}{(2I_a+1)(2I_A+1)} \frac{T_a^{J\pi}(E)\, T_b^{J\pi}(E)}{\sum_c T_c^{J\pi}(E)} \tag{2}$$

Here $T_c^{J\pi}$ are transmission coefficients gotten from optical model potentials, and J, π are the spin and parity of the compound nucleus. Pre-equilibrium emission is included using the intermediate and higher energies, exciton

model, where the energy-dependent cross section is given by:

$$\sigma_{\mathrm{PE}}(E) = \sum_n P(n,E)\sigma_n(E) \tag{3}$$

Here, $P(n,E)$ represent the occupation probability of an exciton configuration, $n = p + h$, and $\sigma_n(E)$ is the emission probability from that configuration.

The EMPIRE implemented four pre-equilibrium approaches: the Multi-Step Direct Model (MSD), the Multi-Step Compound Model (MSC), the PCROSS Exciton Model, and the Hybrid Monte Carlo Simulation approach (HMS).

2.1. Multi-Step Direct (MSD) Model in EMPIRE 3.2

The statistical Multi-Step Direct (MSD) approach in EMPIRE is based on pre-equilibrium scattering to the continuum theory proposed by Tamura, Udagawa, and Lenske [20].

MSD theory employs a combination of Direct Reaction, microscopic nuclear structure, and statistical methods. The effective Hamiltonian H within the EMPIRE framework is presented as:

$$H = H^{opt} + H^{intr} + V^{res} \tag{4}$$

where each term has a distinct physical role in the reaction dynamics.

The optical model Hamiltonian H^{opt} represents the motion of the incident particle in an average complex potential generated by the target nucleus. It accounts for elastic scattering as well as absorption into non-elastic channels and defines the initial interaction stage of the reaction.

The intrinsic Hamiltonian, H^{intr}, describes the internal structure of the target nucleus and can be formulated within the shell model framework, where nucleons occupy discrete energy levels. It can be written as:

$$H^{intr} = H_0^{intr} + V^{intr} \tag{5}$$

where H_0^{intr} corresponds to the independent particle motion in a mean-field potential, while V^{intr} represents the effective nucleon–nucleon interaction responsible for coupling between different particle–hole configurations.

This interaction governs the equilibration process characteristic of the Multi-Step Direct (MSD) mechanism.

The residual interaction V^{res} provides the coupling between the projectile motion and the intrinsic excitations of the nucleus. It drives transitions between channels of increasing complexity and is accountable for particle–hole states during the Multi-Step Direct (MSD) process. In this context, V^{res} acts as the transition operator linking successive stages of the reaction, while V^{intr} governs the mixing and redistribution of strength within the intrinsic system.

The assumption is that the mixing configuration stochastically exists between classes of $np - nh$ in nature, which is randomly distributed in amplitude with a mean value of zero [21].

The probability of finding an energy system within the given configuration can be written as spectroscopic densities.

$$P_c(E) = -\frac{1}{\pi} Im\left[\int dE^1 g(E - E^1)(c\left|G^{intr}\left(E^1\right)\right|c)\right] \tag{6}$$

$P_c(E)$ is spectroscopic density, representing the probability of populating a configuration c at excitation energy E, $G^{intr}(E)$ is the intrinsic Green's function, describing the propagation of the system within the space of intrinsic (particle–hole) configurations, $(c\left|G^{intr}\left(E^1\right)\right|c)$ represent the diagonal matrix element of the Green's function for the configuration c, giving the response of that configuration at energy E, Im is the imaginary part, which ensures that the expression corresponds to a physical density of states, $g(E - E^1)$ is an energy averaging (or smoothing) function, typically introduced in the EMPIRE formalism to account for finite energy resolution and to smooth fluctuations in the discrete spectrum, and E^1 is intermediate excitation energy over which the intrinsic response is integrated.

Furthermore, the energy-averaged population operator is written as:

$$\hat{P}(E) = \int dE^1 g(E - E^1)\hat{P}_{micro}(E) \tag{7}$$

Where $\hat{P}(E)$ is an energy-averaged population operator, $\hat{P}_{micro}(E)$ is a microscopic population operator defined in the discrete intrinsic configuration space, and $g(E - E^1)$ is a smoothing function, ensuring a continuous representation of the population distribution.

While at energy E, the total level density is:

$$\hat{P}_n(E) = \sum\nolimits_{C=[npnh]} |c)P_c(E)(c| \tag{8}$$

gives the $npnh$ states of a partial level, and where $\hat{P}_n(E)$ represents the total density of accessible nuclear states at energy E.

2.2. Multi-Step Compound (MSC) Model

The Multi-Step Compound (MSC) follows the formalism of Nishioka [22]. In this approach, the equilibration of the composite nucleus is described by a series of transitions through closed channels, categorized into classes based on the number of excitons. Therefore, the sum of the excited particle-hole pair number (n) and the incoming nucleon or excitons was defined in terms of classes (i.e., the number of exciton N for nucleon-induced reactions is given by $N = 2n + 1$). Thus, the expectation cross section of MSC that proceeds from the incident channel a to the exit channel b of the intermediate state is summed over the spins and parities and is written as:

$$\frac{d\sigma_{ab}}{dE} = (1 + \delta_{ab}) \sum T_n^a \pi_{n,m} T_m^b \tag{9}$$

Where $\frac{d\sigma_{ab}}{dE}$ is the differential cross-section for the transition from the incident channel a to exit the channel b, δ_{ab} represent the Kronecker delta, accounting for identical entrance and exit channels, n, m denote the indices labelling classes of intrinsic nuclear configurations (e.g., particle–hole excitations), T_n^a is the transmission coefficient describing the coupling of the incident channel a to configuration class n, T_m^b represent the transmission coefficient for decay from the configuration class m into the exit channel b and $\pi_{n,m}$ is the propagation (or transition) probability between configuration classes n and m, representing the internal evolution of the system.

The transmission coefficient T_n^a describes the coupling between classes n and channel a is written as:

$$T_n^a = \frac{4\pi^2 U_n^a}{(1 + \pi^2 \sum_m U_m^a)^2} \tag{10}$$

Here U_n^a is the coupling strength between channels a and configuration class n. The coupling term $U_n^a = \rho_n^b \langle W_{n,a} \rangle$ is microscopically defined in terms of ρ_n^b and $W_{n,a}$ and ρ_n^b is the average bound level density of class n, $W_{n,a}$ is the average matrix element connecting channel a with the states in class n.

2.3. The PCROSS Exciton Model

The PCROSS exciton module includes the pre-equilibrium mechanism, which is defined in the exciton model incorporated in the master equation in the form proposed by Cline [23] and Ribanský et al. [24]. Which can be written as:

$$-q_{t=0}(n) = \lambda_+(E, n+2)\tau(n+2) + \lambda_-(E, n-2)\tau(n-2) - [\lambda_+(E, n) + \lambda_-(E, n) + L(E, n)]\tau(n) \tag{11}$$

where $-q_{t=0}(n)$ is the initial occupation probability of the composite nucleus in the state with the exciton number n, $\lambda_+(E, n)$ and $\lambda_-(E, n)$ are the transition rates for the decay to neighboring states and $L(E, n)$ represent the total emission rate integrated over emission energy for particles including protons (π), neutron (υ) clusters, and γ rays.

2.4. Hybrid Monte Carlo Simulation (HMS) Pre-Equilibrium Model

The Hybrid Monte Carlo Simulation (HMS) approach to the pre-equilibrium emission of a nucleus is inspired by a hybrid model version of the Intra-Nuclear Cascade [25]. It treats all excitons, including holes, on equal footing, giving each of them a chance to interact or to be emitted with a priori equal probability and ending the cascade when all excitons are bound. For an incident neutron, we have P_{nn} as the probability of exciting a neutron given as:

$$P_{nn} = \frac{(A - Z)}{(A - Z) + 3Z} \tag{12}$$

While P_{np} as the probability of exciting a proton is given as:

$$P_{np} = 1 - P_{nn} \tag{13}$$

Similarly, for an incident proton, we have:

$$\begin{aligned} P_{pp} &= \frac{Z}{Z + 3(A - Z)} \\ P_{pn} &= 1 - P_{pp} \end{aligned} \tag{14}$$

The factors of 3 in Equations (12)–(14) arise from the statistical weighting associated with the relative transition probabilities between neutron and proton states, reflecting the underlying nucleon–nucleon interaction asymmetry in the exciton model.

The energy distribution of the scattered particle $P(\varepsilon)$ when n = 2 or 3 is given as:

$$P(\varepsilon) = \frac{\rho_{n-1}(E - \varepsilon)g}{\rho_n(E)} d\varepsilon \tag{15}$$

Here, where V is the Potential well depth,

$$\begin{aligned} \rho_2(E) &= g(gV)/2 \text{ if } E > V; \\ \rho_2(E) &= g(gE)/2 \text{ if } E \leq V \end{aligned} \tag{16}$$

and

$$\rho_3(E) = g^3[V(2E - V)/4 \text{ if E} \geq V. \tag{17}$$

The emission probability $P_v(E)$ is calculated as:

$$P_v(E - Q) = \frac{\lambda_c(\varepsilon - Q)}{\lambda_c(\varepsilon - Q) + \lambda_+(\varepsilon)} \tag{18}$$

Where the emission rate $\lambda_c(\varepsilon - Q)$ is given as:

$$\lambda_c(\varepsilon - Q) \sim \frac{\sigma_v(\varepsilon - Q)(\varepsilon - Q)(2S + 1)\mu_v}{g} \tag{19}$$

Here, σ_v is the inverse reaction cross section, Q is the binding energy, g is the single particle density, S is the nucleon Spin, μ_v is the reduced nucleon mass, and $\lambda_+(\varepsilon)$, the transition rate is calculated from the mean free path of a nucleon in nuclear matter according to the hybrid model.

3. Results and Discussions

Calculated excitation functions were compared directly with available experimental data without normalization. Energy-dependent deviations were analysed to link model performance to the relative strength of contribution to pre-equilibrium mechanisms.

This concise approach enables a transparent assessment of how EMPIRE 3.2.3 model assumptions influence neutron-induced reaction cross sections on Sulphur and chlorine isotopes.

The results of ^{32}S(n,p)^{32}P cross-section are presented in **Figure 1**. These became significant around 2 MeV, with the cross section rising steeply from 0.30 to 3.5 barns within the neutron energy range from 2 MeV to 5 MeV. The differences among the EMPIRE 3.2.3 model options (MSD, MSC, PCROSS, and HMS) at a neutron incident energy of 8 MeV may arise from the distinct treatments of pre-equilibrium emission and collective nuclear effects as implemented in each model option. The MSD calculation shows a smooth increase in the cross section and begins to fall at an incident energy of 9 MeV. The MSC model suppressed the reaction strength in the 9 MeV energy region, which may arise mainly from faster damping of collective enhancements in the level density at high excitation energies. In contrast, the PCROSS and HMS increase the probability of emission of a proton by enhancing the evolution of exciton and nucleon mean free paths by delaying the cross-section falloff at higher energies at about 15 MeV. As a

result, the spreading of the cross section reflects how each model's partition between the decay of the compound nucleus and the preequilibrium process.

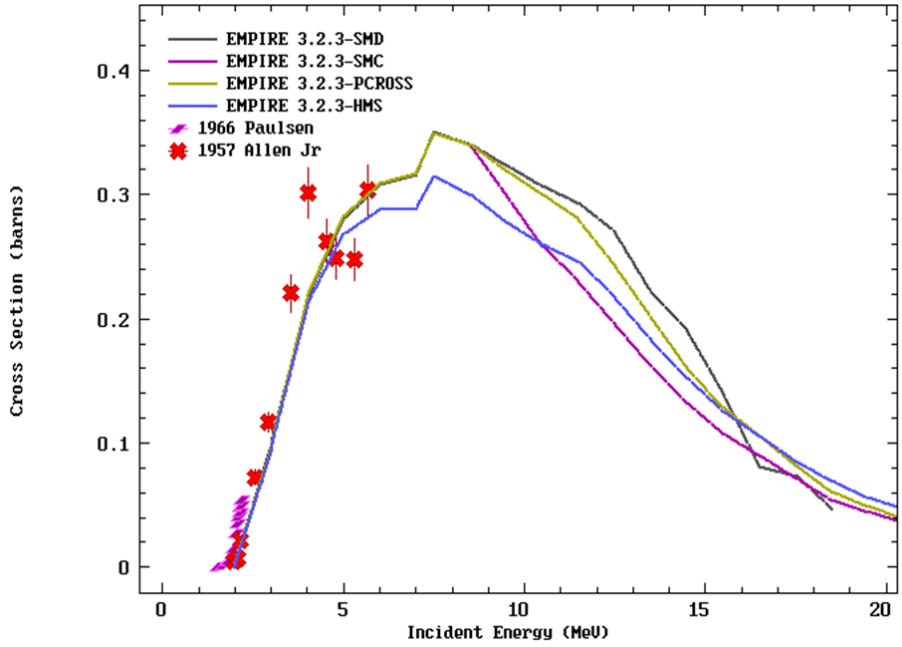

Figure 1. Excitation functions for $^{32}S(n,p)^{32}P$ reaction using the EMPIRE 3.2.3 code with MSD, MSC, PCROSS, and HMS model options, compared with available experimental data.

Predicted results are compared with the available experimental data of Allen et al. (1957) [26] and Paulsen and Liskien (1966) [27]. The MSD, MSC, PCROSS, and HMS model options are consistent with the trend of measured cross sections up to 5 MeV, while the HMS falls off with reduced pre-equilibrium contributions between 5–10 MeV. Additionally, MSC and PCROSS calculations were observed to maintain higher cross sections that decrease more gradually with increasing incident energy. This behaviour suggests that, at higher incident energies, MSC pre-equilibrium processes remain significant for the $^{32}S(n,p)^{32}P$ reaction. The observed agreements and discrepancies between the models and the measurements can be ascribed to differences in the prescription of level-density and exciton dynamics. These results underline the sensitivity of (n,p) reaction modelling inputs and highlight the importance of carefully selecting or constraining model parameters in data evaluation work.

Figure 2 presents the excitation function of the $^{35}Cl(n,\alpha)^{32}P$ reaction. The observed differences among the pre-equilibrium model options (MSD, MSC, PCROSS, and HMS) is subtle but consistent with the conservative level-density parameterizations and reduced strength of collective enhancements. While modest predictions with higher values were observed in PCROSS and HMS options because of the inclusion of more detailed multistep compound and multistep direct contributions, enhancing the probability of gamma-emission following higher exciton configurations.

The results of the reaction cross section of $^{35}Cl(n,\alpha)^{32}P$ were compared with the experimental data from the EXFOR [28]. It can be observed that the theoretical predictions from the MSD, MSC, PCROSS, and HMS models generally align with the experimental data from Batchelder et al. (2019) [17], Kuvin (2020) [18], Sansarbayar et al. (2021) [2], and Hanselman et al. (2024) [29]. Most experimental points lie close to or slightly above the model curves, indicating reasonable agreement across the energy range. The logarithmic scale emphasizes the wide variation in cross-section values, so small deviations are visually less pronounced, but the overall trend shows that the models capture the behavior of the experimental data. The dense cluster of data points at energies between 5–10 MeV, where data points cluster densely, MSC exhibits the closest agreement with the experimental data, confirming that the active multistep gamma-emission channels are important in this reaction. At energies above 10 MeV, all EMPIRE options converge and decline consistently, showing no strong high-energy enhancement.

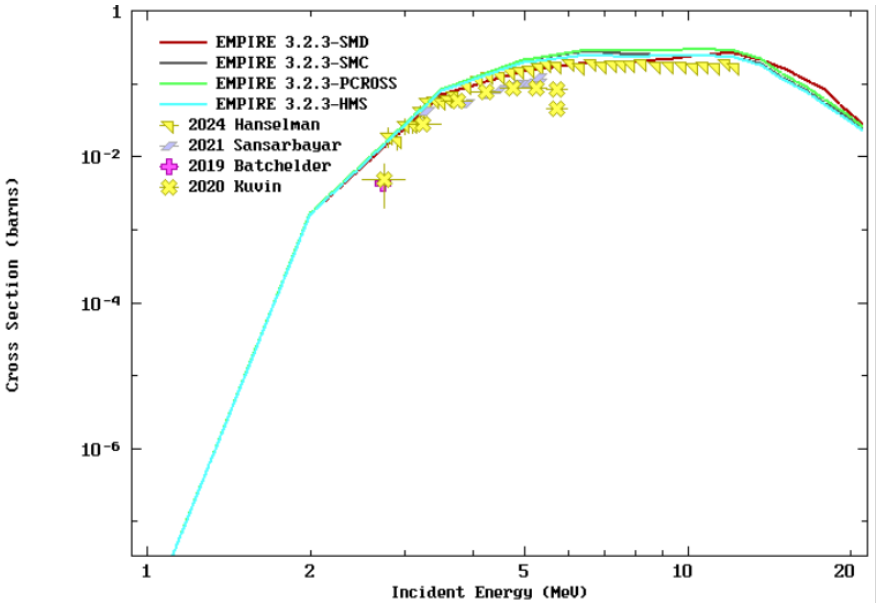

Figure 2. Excitation functions for $^{35}Cl(n,\alpha)^{32}P$ reaction using the EMPIRE 3.2.3 code with MSD, MSC, PCROSS, and HMS model options, compared with available experimental data.

Figure 3 presents the excitation function of the $^{35}Cl(n,p)^{35}S$ reaction. The model options of EMPIRE 3.2.3 (MSD, MSC, PCROSS, and HMS) display a broadly similar behaviour, but differences appear near and above the reaction peak cross section of 0.2 b at neutron incident energy of 8–12 MeV. At low energies (<2 MeV), all models closely overlap because the reaction is dominated by compound nucleus formation, where the level density prescription and pre-equilibrium effects have minimal influence. As the incident energy increases, MSD, MSC, and PCROSS curves tend to remain slightly higher than HMS predictions as the incident energy increases above 5 MeV. The difference arises due to MSD and MSC employing more conservative level-density and optical-model treatments, which consequently reduces the contribution of the pre-equilibrium proton emission. These shapes produce a higher cross-section and a broader cross-section peak in the 8–12 MeV region for MSD and MSC.

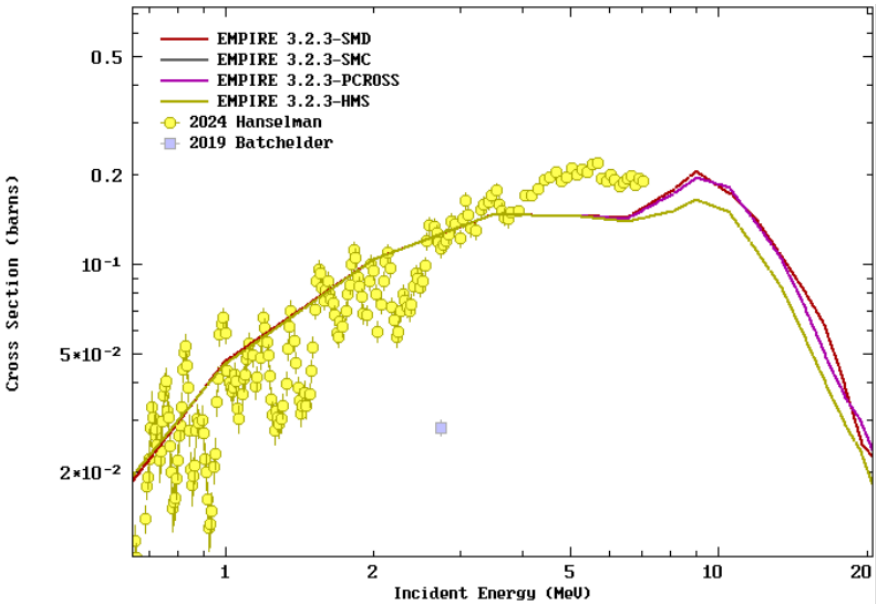

Figure 3. Excitation functions for $^{35}Cl(n,p)^{35}S$ reaction using the EMPIRE 3.2.3 code with MSD, MSC, PCROSS, and HMS model options, compared with available experimental data.

The assumptions of the underlying physical models directly influence the level of agreement with experimental data. The recent measurements of Hanselman et al. (2024) [29] show good agreement with the pre-equilibrium model predictions (MSD, MSC, PCROSS, and HMS) up to 5 MeV, indicating that pre-equilibrium processes play a significant role in proton emission. All EMPIRE pre-equilibrium options exhibit a peak approximately between 8 and 9 MeV in **Figure 3**, followed by a similar decline. In contrast, the earlier data from Batchelder et al. (2019) [17] lie noticeably below both the main cluster of experimental data and the model predictions, while the results of Hanselman et al. (2024) [29] suggest a possible outlier rather than a systematic physical deviation.

The energy-dependent differences among the EMPIRE 3.2.3 model options arise from variations in level-density formulations, optical-model transmission coefficients, and the treatment of pre-equilibrium processes.

Table 1 presents the peak energy corresponding to the peak cross-section values in the reaction channel for $^{32}S(n,p)^{32}P$, $^{35}Cl(n,a)^{32}P$, and $^{35}Cl(n,p)^{35}S$. This demonstrates the influence of the Preequilibrium model options in the EMPIRE 3.2.3 code. The highest peak cross section was observed in the PCROSS option, indicating sensitivity of $^{32}S(n,p)^{32}P$, $^{35}Cl(n,a)^{32}P$ reaction to the evolution of exciton and emission of the charge particle at an intermediate.

Table 1. Peak Energies Correspond to Peak Cross Sections for the Studied Reactions.

Reaction	Peak Energy (MeV)	Peak Cross Section (barns)			
		SMD (barns)	SMC (barns)	PCROSS (barns)	HMS (barns)
$^{32}S(n,p)^{32}P$	7–9	0.34983	0.34922	0.34922	0.31491
$^{35}Cl(n,a)^{32}P$	10–12	0.26385	0.25428	0.31430	0.24849
$^{35}Cl(n,p)^{35}S$	8–10	0.20467	0.16407	0.19479	0.16407

In contrast, the $^{35}Cl(n,p)^{35}S$ reaction has its peak cross section between 8–10 MeV, with the MSD exceeding PCROSS. This suggests that the sensitivity of MSD for the $^{35}Cl(n,p)^{35}S$ reaction is much stronger than compared to the other preequilibrium models' options. **Table 1** indicates that, for the reactions considered in this study, the PCROSS contribution tends to increase the peak cross section; in contrast, MSD, MSC, and HMS yield relatively conservative peak estimates, particularly for reactions dominated by compound-nucleus decay. However, a quantitative measure of how different model assumptions influence reaction output is provided in **Table 1**, which supports the importance of selecting an appropriate model for accurate nuclear data evaluation.

4. Conclusions

This study compared pre-equilibrium model options in the EMPIRE 3.2.3 code (MSD, MSC, PCROSS, and HMS) against experimental data for the reactions $^{32}S(n,p)^{32}P$, $^{35}Cl(n,\alpha)^{32}P$, and $^{35}Cl(n,p)^{35}S$. As reflected in **Figure 2**, all model options reproduce the general shape of the excitation functions, showing a gradual increase in cross section up to a peak around 8–10 MeV, followed by a decline at 10–20 MeV.

At incident energies from threshold to 5 MeV, the close overlap of all model predictions and their agreement with experimental data in **Figures 1–3** indicate that compound nucleus contributions are dominant and reasonably well constrained. As the energy increases, small but noticeable deviations among the model options emerge, consistent with differences in the treatment of pre-equilibrium emission.

Overall, the experimental data are reasonably well reproduced by all models within the observed scatter, with no single model showing consistent superiority across the entire energy range. The results highlight the sensitivity of calculated cross sections to the choice of pre-equilibrium model, particularly in the energy region where pre-equilibrium effects become more relevant. These findings provide useful guidance for model selection in nuclear reaction calculations involving sulphur and chlorine isotopes.

Author Contributions

Simulation, A.B.O.; supervised and proofread, A.M.E.; original draft preparation, D.A.A.; review and editing, M.A. and M.I.A. All authors have read and agreed to the published version of the manuscript.

Funding

This work received no external funding.

Institutional Review Board Statement

Not applicable.

Informed Consent Statement

Not applicable.

Data Availability Statement

The data supporting the findings of this study are available within the article and the data obtained from publicly available databases are properly cited in the manuscript.

Acknowledgments

The authors gratefully acknowledge the International Atomic Energy Agency (IAEA) for making the EMPIRE 3.2.3 code available for use and for providing access to the EXFOR nuclear reaction database used in this study.

Conflicts of Interest

The authors declare that they have no known competing financial interests or personal relationships that could have appeared to influence the work reported in this paper.

AI Use Statement

No artificial intelligence (AI) tools were used in the preparation of this manuscript.

References

1. Olorunsola, A.; Bamikole, J.; Bello, A.; et al. Theoretical Prediction of Neutron-Induced Radiative Capture Cross Section of Some Isotopes of Minor Actinides. *J. Nucl. Radiat. Sci.* **2023**, *2*, 1.
2. Sansarbaya, E.; Gledenov, Y.M.; Chuprakov, I.; et al. Cross Section for the ^{35}Cl(n,α)^{32}P Reaction in the 3.3–5.3 MeV Neutron Energy Region. *Phys. Rev. C* **2021**, *104*, 044620.
3. Ige, O.O.; Olorunsola, A.B.; Adoyi, E.I.; et al. Cross-Section Calculations and Comparative Assessment of Al and Zr as Cladding for NIRR-1. *Math. Model. Eng. Probl.* **2024**, *11*, 2680–2656.
4. Luo, J.; He, L.; Zhou, L.; et al. Determination of Cross Sections for the ^{80}Kr(n,2n)^{79}Kr Reaction in the Neutron Energy Range of 13–15 MeV. *Chin. Phys. C* **2025**, *49*, 084005.
5. Herman, M.; Capote, R.; Carlson, B.; et al. EMPIRE: Nuclear Reaction Model Code System for Data Evaluation. *Nucl. Data Sheets* **2007**, *108*, 2655–2715.
6. Koning, A.J.; Hilaire, S.; Goriely, S. TALYS: Modeling of Nuclear Reactions. *Eur. Phys. J. A* **2023**, *59*, 131.
7. Kawano, T. CoH3: The Coupled-Channels and Hauser–Feshbach Code. In Proceedings of the 6th International Workshop on Compound-Nuclear Reactions and Related Topics (CNR*18), Berkeley, CA, USA, 24–28 September 2018; pp. 27–34.
8. Jalili, A.; Pan, F.; Chen, A.X.; et al. Multilayer perceptron for fission yield predictions: A physics-guided approach. *Phys. Rev. C* **2026**, *113*, 034605.
9. Olorunsola, A.B.; Bamikole, J.A.; Bello, A.A. Statistical Analysis of Neutron-Induced Capture Cross Section in Some Isotopes of Plutonium Using EMPIRE 3.2 Code. *IOSR J. Appl. Phys.* **2023**, *15*, 28–36.
10. Hauser, W.; Feshbach, H. The Inelastic Scattering of Neutrons. *Phys. Rev.* **1952**, *87*, 366–373.
11. Olorunsola, A.B.; Bamikole, J.A.; Bello, A.A.; et al. Model Calculation and Evaluation of Neutron-Induced Reaction Cross Section on ^{237}Np, ^{241}Am, and ^{245}Cm Using the EMPIRE 3.2 Code. *AIP Conf. Proc.* **2023**, *2754*, 030010.
12. Carlson, B.V.; Herman, M.; Rego, M.E.; et al. Exclusive Multiple Emission Cross Sections in the Hybrid Monte Carlo Preequilibrium Model and in EMPIRE-3.1. *Nucl. Data Sheets* **2014**, *118*, 276–279.
13. Galanopoulos, S.; Vlastou, R.; Demetriou, P.; et al. Statistical Model Calculations of ^{72,74}Ge(n,p) and ^{72,74}Ge(n,α) Reactions on Natural Ge. *HNPS Adv. Nucl. Phys.* **2020**, *15*, 104–110.
14. Olorunsola, A.B.; Ige, O.O.; Ayemowa, M.O.; et al. Study of Optimal Model and Parameters of the Th–U Cycle Nuclei. *Energy Storage Sav.* **2026**, in press. [CrossRef]

15. Al-Abyad, M.; Spahn, I.; Sudár, S.; et al. Nuclear data for production of the therapeutic radionuclides ^{32}P, ^{64}Cu, ^{67}Cu, ^{89}Sr, ^{90}Y and ^{153}Sm via the (n,p) reaction: Evaluation of excitation function and its validation via integral cross-section measurement using a 14 MeV d(Be) neutron source. *Appl. Radiat. Isot.* **2006**, *64*, 717–724.
16. Soltani-Farshi, M.; Meyer, J.D.; Misaelides, P.; et al. Cross Section of the ^{32}S(α,p)^{35}Cl Nuclear Reaction for Sulphur Determination. *Nucl. Instrum. Methods Phys. Res. B* **1996**, *113*, 399–402. [CrossRef]
17. Batchelder, J.C.; Chong, S.A.; Morrell, J.; et al. Possible Evidence of Nonstatistical Properties in the ^{35}Cl(n,p0)^{35}S Cross Section. *Phys. Rev. C* **2019**, *99*, 044612.
18. Kuvin, S.A.; Lee, H.Y.; Kawano, T.; et al. Nonstatistical Fluctuations in ^{35}Cl(n,p)^{35}S Reaction Cross Section at fast-neutron energies from 0.6 to 6 MeV. *Phys. Rev. C* **2020**, *102*, 024623.
19. Raynal, J. Optical-Model and Coupled-Channel Calculations in Nuclear Physics. In *ICTP International Seminar Course*; IAEA/ICTP: Trieste, Italy, 1979; p. 281.
20. Tamura, T.; Udagawa, T.; Lenske, H. Multistep direct reaction analysis of continuum spectra in reactions induced by light ions. *Phys. Rev. C* **1982**, *26*, 379.
21. Lenske, H.; Wolter, H.H. Statistical Direct Reaction Theory for Dissipative Heavy Ion Collisions. *Nucl. Phys. A* **1992**, 483–490.
22. Nishioka, H. Statistical Theory of Nuclear Reactions: Comparisons with Unimolecular Reactions and Microcluster Productions. *Prog. Theor. Phys. Suppl.* **1994**, *116*, 451–456.
23. Cline, C.K. Extensions to the pre-equilibrium statistical model and a study of complex particle emission. *Nucl. Phys. A* **1972**, *193*, 417–437.
24. Ribanský, E.; Obložinský, P.; Beták, E. Pre-Equilibrium Decay and the Exciton Model. *Nucl. Phys. A* **1973**, *205*, 545–560.
25. Blann, M.; Mignerey, A. Pre-Equilibrium Decay at Moderate Excitations. *Nucl. Phys. A* **1972**, *186*, 245–256.
26. Allen, L.; Bigger, W.A.; Prestwood, R.J.; et al. Cross Sections for ^{32}S(n,p)^{32}P and ^{34}S(n,α)^{31}Si Reactions. *Phys. Rev.* **1957**, *107*, 1363.
27. Paulsen, A.; Liskien, H. Cross Sections for Some (n,p) Reactions Near Threshold. In Proceedings of the Conference on Nuclear Data for Reactors: Nuclear Data, Microscopic Cross Sections and Other Data Basic for Reactors, Paris, France, 17–21 October 1966; pp. 217–224. Available online: https://www.osti.gov/biblio/4551955-cross-sections-some-reactions-near-threshold?utm_
28. Otuka, N.; Dupont, E.; Semkova, V.; et al. EXFOR: Experimental Nuclear Reaction Data Library. *Nucl. Data Sheets* **2014**, *120*, 272.
29. Hanselman, K.; Kuvin, S.A.; Lee, H.Y.; et al. Improved Modelling of Neutron-Induced Reactions on Chlorine Isotopes Aided through New (n,p) and (n,α) Measurements at LANSCE. *Phys. Rev. C* **2024**, *110*, 024609.